Drivers of heterogeneity in tundra vegetation productivity on the Yamal Peninsula, Siberia, Russia

ENVIRONMENTAL RESEARCH
ECOLOGY

OPEN ACCESS

RECEIVED
14 September 2023

REVISED
4 January 2024

ACCEPTED FOR PUBLICATION
24 January 2024

PUBLISHED
14 February 2024

PAPER

Drivers of heterogeneity in tundra vegetation productivity on the Yamal Peninsula, Siberia, Russia

Morgan S Tassone[1,*], Howard E Epstein[1], Amanda H Armstrong[1,2], Uma S Bhatt[3], Gerald V Frost[4], Birgit Heim[5], Martha K Raynolds[6] and Donald A Walker[6]

[1] Department of Environmental Sciences, University of Virginia, Charlottesville, VA, United States of America
[2] Universities Space Research Association, Columbia, MD, United States of America
[3] Geophysical Institute, University of Alaska Fairbanks, Fairbanks, AK, United States of America
[4] Alaska Biological Research, Inc., Fairbanks, AK, United States of America
[5] Research Unit Potsdam, Alfred-Wegener-Institut Helmholtz-Zentrumfür Polar-und Meeresforschung, Potsdam, Germany
[6] Institute of Arctic Biology, University of Alaska Fairbanks, Fairbanks, AK, United States of America
[*] Author to whom any correspondence should be addressed.

E-mail: mms3sh@virginia.edu

Keywords: normalized difference vegetation index, moderate resolution imaging spectroradiometer, Arctic, tundra, vegetation, productivity

Supplementary material for this article is available online

Abstract

The direction and magnitude of tundra vegetation productivity trends inferred from the normalized difference vegetation index (NDVI) have exhibited spatiotemporal heterogeneity over recent decades. This study examined the spatial and temporal drivers of Moderate Resolution Imaging Spectroradiometer Max NDVI (a proxy for peak growing season aboveground biomass) and time-integrated (TI)-NDVI (a proxy for total growing season productivity) on the Yamal Peninsula, Siberia, Russia between 2001 and 2018. A suite of remotely-sensed environmental drivers and machine learning methods were employed to analyze this region with varying climatological conditions, landscapes, and vegetation communities to provide insight into the heterogeneity observed across the Arctic. Summer warmth index, the timing of snowmelt, and physiognomic vegetation unit best explained the spatial distribution of Max and TI-NDVI on the Yamal Peninsula, with the highest mean Max and TI-NDVI occurring where summer temperatures were higher, snowmelt occurred earlier, and erect shrub and wetland vegetation communities were dominant. Max and TI-NDVI temporal trends were positive across the majority of the Peninsula (57.4% [5.0% significant] and 97.6% [13.9% significant], respectively) between 2001 and 2018. Max and TI-NDVI trends had variable relationships with environmental drivers and were primarily influenced by coastal-inland gradients in summer warmth and soil moisture. Both Max and TI-NDVI were negatively impacted by human modification, highlighting how human disturbances are becoming an increasingly important driver of Arctic vegetation dynamics. These findings provide insight into the potential future of Arctic regions experiencing warming, moisture regime shifts, and human modification, and demonstrate the usefulness of considering multiple NDVI metrics to disentangle the effects of individual drivers across heterogeneous landscapes. Further, the spatial heterogeneity in the direction and magnitude of interannual covariation between Max NDVI, TI-NDVI, and climatic drivers highlights the difficulty in generalizing the effects of individual drivers on Arctic vegetation productivity across large regions.

1. Introduction

Arctic vegetation plays a critical role in global climate feedbacks (Pearson *et al* 2013), permafrost dynamics (Blok *et al* 2010), and the distribution of herbivore populations connected to the livelihood of Arctic communities (Forbes and Kumpula 2009). Changes in Arctic vegetation since the 1980s have been

monitored using the normalized difference vegetation index (NDVI) (Frost *et al* 2021), a proxy for primary productivity that remotely quantifies photosynthetically-active green vegetation (Reichle *et al* 2018). While NDVI and Arctic aboveground biomass have been found to have a weakly positive linear relationship ($R^2 = 0.23$) at finer resolutions (<1 km) (Cunliffe *et al* 2020), there is evidence of a strong positive non-linear relationship ($R^2 = 0.94$) between Arctic aboveground biomass and NDVI at coarser resolutions (⩾1 km), allowing in situ vegetation changes to be inferred from NDVI metrics at broader scales (Jia *et al* 2006, Epstein *et al* 2012, Raynolds *et al* 2012). Max NDVI (the greatest intra-annual NDVI value) represents peak growing season aboveground biomass, whereas time-integrated (TI)-NDVI (the sum of growing season NDVI values >0.05) represents total growing season productivity (Jia *et al* 2006, Bhatt *et al* 2021).

Despite net increases in Max NDVI and TI-NDVI since 1982 (Frost *et al* 2020), the direction and magnitude of Arctic vegetation productivity trends exhibit substantial spatiotemporal heterogeneity across multiple scales (e.g. local to continental, inter-annual to decadal) (Elmendorf *et al* 2012, Lara *et al* 2018, Berner *et al* 2020, Myers-Smith *et al* 2020). This spatiotemporal heterogeneity is likely due to complex vegetation interactions with climatic, geomorphic, biologic, and anthropogenic drivers (Walker *et al* 2009, Yu *et al* 2017, Frost *et al* 2021). While some of these relationships are well-studied, there are uncertainties in determining the relative importance of drivers across regions with varying climatological conditions, landscapes, and vegetation communities (Epstein *et al* 2004, Walker 2006, Dutrieux *et al* 2012, Bhatt *et al* 2021).

This study examined the effects of environmental and anthropogenic drivers on the spatial and temporal patterns of vegetation productivity on the Yamal Peninsula, Siberia, Russia (hereafter, the Peninsula) using NDVI metrics derived from Moderate Resolution Imaging Spectroradiometer (MODIS) data. The Peninsula is located in one of the warmer regions of the Arctic (Raynolds *et al* 2008), has steep climate and geomorphic gradients, ice-rich continuous permafrost, diverse Arctic vegetation, extensive indigenous reindeer herding, and burgeoning natural resource (gas) development (figure 1, Walker *et al* 2009). These conditions allowed it to serve as a case study for determining the critical drivers of Arctic vegetation productivity (Macias-Fauria *et al* 2012) under projected warming (IPCC 2021), increasing resource extraction (Walker 2010), and ongoing herbivory. Specifically, this study aimed to determine (1) which drivers exerted the greatest influence on the spatial distribution of Max and TI-NDVI across the Peninsula between 2001 and 2018, (2) the direction and magnitude of the Peninsula's Max and TI-NDVI trends between 2001 and 2018, and (3) which drivers best predicted variations in these trends.

We hypothesized that climatic drivers and physiognomic vegetation unit would best explain the spatial distribution of Max and TI-NDVI because of the influence of long-term climate patterns and growth form-specific physiological requirements on Arctic vegetation distribution (Walker *et al* 2002, Raynolds *et al* 2008). Additionally, we expected that Max and TI-NDVI trends would be positive across a majority of the Peninsula; however, spatial heterogeneity in trend magnitude and direction was expected due to variable climatological and landscape conditions. Lastly, we hypothesized that geomorphic and anthropogenic drivers would best explain variations in Max and TI-NDVI trends due to their ability to mediate the effects of climate on vegetation productivity.

2. Methods

2.1. Study area

The Peninsula is located within the Arctic tundra of northwestern Siberia, Russia and is approximately 600 km long (south–north, including Belyy Island in the north) and up to 250 km wide (Walker *et al* 2009). Between 2001 and 2018, the mean annual temperature ranged from −13 °C to −8 °C (Wan *et al* 2015), and mean annual precipitation ranged from 240 to 367 mm (Abatzoglou *et al* 2018). The Peninsula has predominantly flat topography (figure 1), with a majority of slopes < 7°, and elevations reaching 86 m above sea level (Leibman *et al* 2014, Rizzoli *et al* 2017). The landscape is underlain by ice-rich continuous permafrost and dominated by river networks, sandy ridges, and lowland valleys with abundant thermokarst lakes, drained thermokarst lake basins, and polygonal peatlands (Walker *et al* 2009, Verdonen *et al* 2020). Cryogenic landslides controlled by active layer depth and soil water content are the primary disturbance process on the Peninsula (Leibman 1995, Macias-Fauria *et al* 2012, Leibman *et al* 2014). Vegetation transitions from erect low shrub tundra in the south to sedge, prostrate dwarf-shrub, and moss tundra in the north (supplementary figure 1, Walker *et al* 2009). Shrubs are present throughout the Peninsula, but increase in abundance from north to south (Epstein *et al* 2021).

2.2. Data sources and pre-processing

This study employed Max and TI-NDVI derived from the MODIS Vegetation Indices product and a suite of climatic, geomorphic, biologic, and anthropogenic drivers (table 1). A lack of quantitative data and exclusion

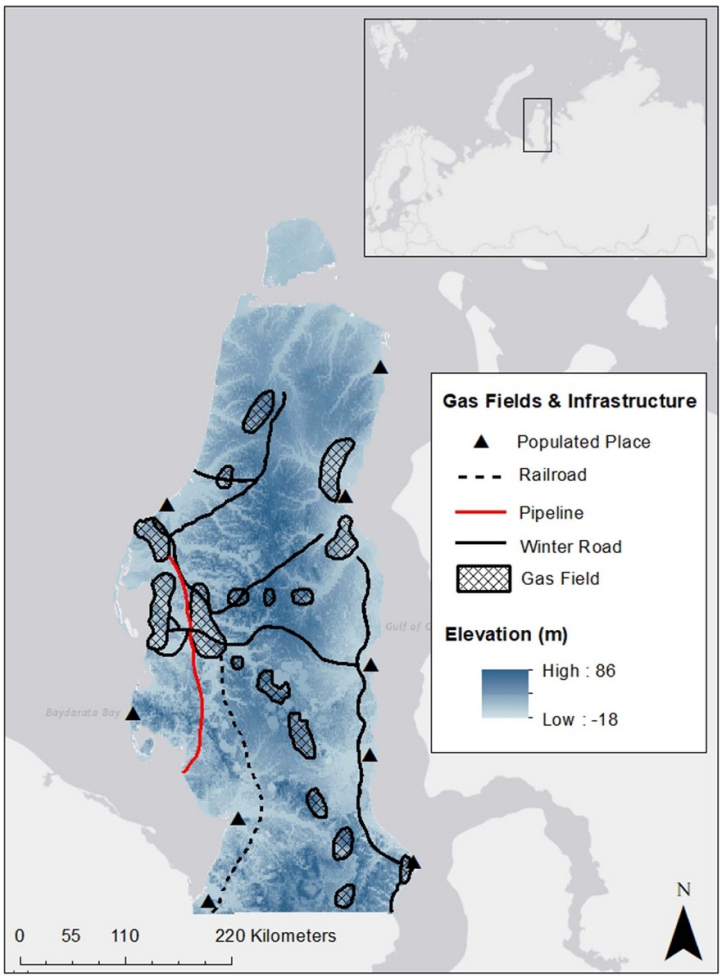

Figure 1. The Yamal Peninsula with elevation (m above sea level) and locations of population centers, infrastructure, and gas fields (Forbes 1999, Gazprom 2021). The inset map shows the location of the Yamal Peninsula.

areas limited the potential for a meaningful assessment of reindeer effects as a biologic driver (Walker *et al* 2009).

Pre-processing was completed using Google Earth Engine (GEE), ArcGIS (Redlands, CA), and R version 4.0.0 (R Core Team 2020). Pre-processing entailed evaluating pixel quality, masking surface water, deriving the parameter of interest for the 2001–2018 study period, and resampling to a 1 km spatial resolution to ensure that the datasets were comparable. Low-quality pixels affected by cloud cover, aerosols, and viewing angle are removed from the operational data products used in this study (FAO/IIASA/ISRIC/ISS-CAS/JRC 2012, Didan 2015, Wan *et al* 2015, Hall *et al* 2016, Rizzoli *et al* 2017, Abatzoglou *et al* 2018, Walker and Raynolds 2018, Kennedy *et al* 2019). Marginal-quality pixels were used to supplement the spatial coverage of snow-free period onset, summer warmth index (SWI), Max NDVI, and TI-NDVI datasets when high-quality data were unavailable. Permanent surface water bodies were masked using the GlobCover Global Land Cover Map (ESA and UC Louvain 2010). A 1 km resolution was used for the analyses because it was the native resolution of the majority of the datasets considered (7 of the 12), which minimized the number of datasets that needed to be resampled (table 1).

2.3. Max and TI-NDVI calculation

The MODIS Vegetation Indices product (MOD13Q1.006) provides NDVI calculated using the equation $(NIR - R)/(NIR + R)$, where NIR equals the reflectance of near-infrared radiation and R equals the reflectance of visible red radiation (Didan 2015). This MODIS product was used because it is comprised of NDVI values derived from 16 day maximum value composite images (hereafter, composites), which allowed for better temporal data quality screening than other available products. The annual Max NDVI for each pixel was determined by selecting the maximum NDVI value from composites covering 26 June–13 September (period of peak vegetation productivity on the Peninsula). Barren, snow-covered, and ephemeral water-covered land surfaces were excluded by masking pixels with Max NDVI values below 0.1 (Raynolds *et al* 2006). Annual TI-NDVI for each pixel was calculated by summing NDVI values above 0.05 from

Table 1. Datasets included in the analyses. *Dependent variables.

Data type	Year(s) included	Dataset(s)	Definition	Native resolution	Source
Continuous	N/A	Distance from the Coast	Kilometers from the coast; considered a proxy for sea ice influence on temperature and precipitation	1 km	Circumpolar Arctic Vegetation Map (Walker and Raynolds 2018)
	N/A	Elevation	N/A	90 m	TanDEM-X 90 m Digital Elevation Model (Rizzoli *et al* 2017)
	2001–2018	Human modification	Cumulative measure of the area impacted by natural resource extraction, infrastructure, and settlements	1 km	Conservation Science Partners (Kennedy *et al* 2019)
	2001–2018	Max NDVI*	Annual peak NDVI value	250 m	Terra MODIS Vegetation Indices (MOD13Q1.006) (Didan 2015)
	2001–2018	Precipitation and soil moisture	Mean snow-free season (April–September) precipitation and soil moisture	2.5 arc minutes	TerraClimate: Monthly Climate and Climatic Water Balance for Global Terrestrial Surfaces, University of Idaho (Abatzoglou *et al* 2018)
	2001–2018	Snow-free period onset	First day of the year with 0% snow cover	500 m	Terra MODIS Snow Cover (MOD10A1.006) (Hall *et al* 2016, Armstrong *et al* 2022)
	2001–2018	Summer warmth index	Sum of April–September monthly mean temperatures >0 °C	1 km	Terra MODIS Land Surface Temperature and Emissivity (MOD11A1.006) (Wan *et al* 2015)
	2001–2018	TI-NDVI*	Annual sum of NDVI values >0.05	250 m	Terra MODIS Vegetation Indices (MOD13Q1.006) (Didan 2015)
Categorical	N/A	Landscape age	Time since last glaciation	1 km	Circumpolar Arctic Vegetation Map (Walker and Raynolds 2018)
	N/A	Physiognomic vegetation unit	N/A	1 km	Circumpolar Arctic Vegetation Map (Walker and Raynolds 2018)
	N/A	Soil texture	N/A	1 km	Circumpolar Arctic Vegetation Map (Walker and Raynolds 2018)
	N/A	Substrate chemistry	N/A	1 km	Circumpolar Arctic Vegetation Map (Walker and Raynolds 2018)

composites covering the entire snow-free season (April–September) (Bhatt *et al* 2021). Each time-period composite included in the Max and TI-NDVI calculations had variable spatial coverage due to the exclusion of low-quality pixels affected by water, clouds, heavy aerosols, and cloud shadows (Didan 2015). Therefore, the number of pixels masked varied for each composite but did not exceed 4.5% for Max NDVI or 12.5% for TI-NDVI. At the pixel scale, this resulted in variable intra-annual coverage and a bias toward artificially low Max and TI-NDVI values. This bias was removed by only calculating annual Max and TI-NDVI for a pixel when data from all time-period composites considered were available. Max and TI-NDVI calculations were completed using GEE.

2.4. Spatial correlations among Max NDVI, TI-NDVI, and continuous drivers

Pairwise Spearman's correlation was used to determine the direction and significance of the spatial relationships among Max NDVI, TI-NDVI, and the continuous drivers (table 1). The 2001–2018 means of Max NDVI, TI-NDVI, and climatic drivers were included as inputs, and all other included variables (coast distance, elevation, and human modification) were constant over the 2001–2018 study period. Although human modification is dynamic, the dataset used here provides a cumulative measure of human modification based on the spatial extent of settlements, agriculture, transportation, mining, energy production, and electrical infrastructure in 2016 (Kennedy *et al* 2019). The Bonferroni correction was applied to account for multiple comparisons. Spearman's correlations were also run on stratified random samples using 2/3 and 1/2 of the input dataset to determine if the results were impacted by spatial autocorrelation. Spearman's correlation was implemented using the psych package in R (R Core Team 2020, Revelle 2020).

2.5. Spatial correlations among Max NDVI, TI-NDVI, and categorical drivers

Chi-square (χ^2) tests of independence were employed to determine if there were significant spatial associations among 2001–2018 mean Max-NDVI, TI-NDVI and categorical drivers (table 1). Mean Max and TI-NDVI were divided into high, mid-, and low categories using the Jenk's natural breaks classification method (implemented using the BAMMtools package in R) (Rabosky *et al* 2014, R Core Team 2020). Chi-square tests of Independence were also run on stratified random samples using 2/3 and 1/2 of the input datasets to determine if the results were impacted by spatial autocorrelation. The χ^2 test statistics and residuals were compared to determine the direction and significance of the spatial associations.

2.6. Trend detection

Mann-Kendall trend tests were implemented to detect the presence of pixel-scale monotonic trends in Max NDVI, TI-NDVI, and climatic drivers between 2001 and 2018. Pixels with fewer than 15 years of data due to the masking of low-quality pixels (described further in section 2.3) were excluded from the analyses (3.9% of the Max NDVI dataset and 4.7% of the TI-NDVI dataset). The Durbin–Watson test found that $<5\%$ of pixels exhibited significant lag-1 serial autocorrelation (Kulkarni and von Storch 1995). Modified Mann–Kendall trend tests were run to verify that pixels with significant serial autocorrelation did not affect trend significance. Sen's slope estimation was used to determine the direction and magnitude of Max NDVI, TI-NDVI, and climatic driver trends. Trend detection analyses were completed using the car (Fox and Weisberg 2019), Kendall (McLeod 2011), modifiedmk (Patakamuri and O'Brien 2020), and trend packages (Pohlert 2020) in R. GEE was used to calculate 2001–2009 and 2010–2018 mean NDVI values for each time-period composite included in the analysis to illustrate shifts in Max NDVI and TI-NDVI between the first and second halves of the study period.

2.7. Drivers of Max and TI-NDVI trends

Random forest regression (RFR) models were used to determine the best predictors of Max and TI-NDVI trends (Sen's slopes) across the Peninsula. All drivers were included as explanatory variables in the models, and the Sen's slopes of climatic drivers were used (table 1). A pairwise Spearman's correlation was used to confirm that multicollinearity ($r > 0.75$ or < -0.75) was not present among the continuous input drivers (Berner *et al* 2020). RFR models were trained using bootstrapped data and tuned to determine the number of randomized drivers considered at each tree node (mtry = 5) that resulted in the lowest mean square error (MSE) (Oliveira *et al* 2012). The mean decrease in accuracy (% IncMSE) metric was used to determine variable importance (Liaw and Wiener 2002). Additional RFR models were run for areas where significant Max and TI-NDVI trends were observed to determine if the best predictors of trends across the Peninsula were also driving change in these areas. RFR modeling was completed using the caret (Kuhn 2020), randomForest (Liaw and Wiener 2002), and doParallel packages (Microsoft and Weston 2020) in R.

The relationships between Max/TI-NDVI trends and the six most important drivers identified by the RFR models were evaluated using partial dependence plots. Pixel-scale Spearman's correlations were run between linearly-detrended Max/TI-NDVI and the three most important climatic driver time series (precipitation, soil moisture, and SWI) to assess their interannual covariation irrespective of trends, and therefore what drove variability in Max and TI-NDVI year to year. Linear detrending was completed by modeling a linear function and then subtracting the function from the observed data. These analyses were completed using the pdp (Greenwell 2017), pracma (Borchers 2019), and psych packages (Revelle 2020) in R.

3. Results

3.1. Continuous spatial drivers of Max and TI-NDVI

Correlations between time-averaged parameters over the 2001–2018 study period were evaluated to determine the strength of their spatial relationships. There was a significant (p-value < 0.05), strong, and positive spatial correlation between mean Max and TI-NDVI ($r = 0.93$, figure 2 and supplemental figure 2). Mean Max NDVI exhibited the strongest significant spatial correlations with mean SWI ($r = 0.40$), mean precipitation ($r = 0.39$), and mean snow-free period onset date ($r = -0.40$), as well as weaker but significant correlations with the other continuous drivers (except for elevation). Mean Max NDVI was positively correlated with human modification ($r = 0.27$) and weakly correlated with mean soil moisture ($r = 0.02$) and coast distance ($r = -0.02$). Therefore, areas with higher Max NDVI coincided with higher SWI, higher precipitation, earlier snowmelt, and higher human modification, whereas Max NDVI exhibited little to no spatial relationship with soil moisture, coast distance, or elevation. Mean TI-NDVI exhibited similar spatial relationships with the continuous drivers; however, mean TI-NDVI was not significantly correlated with mean soil moisture, and was better correlated with mean SWI, mean precipitation, mean snow-free period onset date, human modification, coast distance, and elevation than mean Max NDVI (figure 2). Results were similar for analyses run on stratified random samples using 2/3 and 1/2 of the input dataset.

Notable spatial correlations among the continuous drivers were present. Mean precipitation was positively correlated with mean SWI ($r = 0.89$), and both mean precipitation and mean SWI were negatively correlated with mean snow-free period onset date ($r = -0.86$ and -0.85, respectively; figure 2 and supplemental figure 3). Human modification was positively correlated with mean SWI ($r = 0.32$) and mean precipitation ($r = 0.47$), and negatively correlated with mean snow-free period onset date ($r = -0.44$); therefore, on average, human settlement more frequently coincided with higher SWI, higher precipitation, earlier snowmelt. Additionally, coast distance was positively correlated with elevation ($r = 0.63$) and mean SWI ($r = 0.40$), and negatively correlated with mean soil moisture ($r = -0.72$), indicating that mean elevation and SWI increased with distance from the coast while soil moisture decreased.

3.2. Categorical spatial drivers of Max and TI-NDVI

Vegetation unit had the strongest spatial association with mean Max NDVI categories ($\chi^2 = 10\,674$), followed by substrate chemistry ($\chi^2 = 5672$), soil texture ($\chi^2 = 2337$), and landscape age ($\chi^2 = 128$). Similarly, vegetation unit had the strongest spatial association with mean TI-NDVI categories ($\chi^2 = 25\,903$), followed by soil texture ($\chi^2 = 3747$), substrate chemistry ($\chi^2 = 2966$), and landscape age ($\chi^2 = 1748$). High mean Max and TI-NDVI were associated with erect shrub and wetland vegetation (a combination of sedges, mosses, and erect shrubs) (Raynolds *et al* 2006), whereas low mean Max and TI-NDVI were associated with graminoid and prostrate shrub vegetation. High mean Max and TI-NDVI were associated with circumneutral substrates, whereas low mean Max and TI-NDVI were associated with acidic and saline substrates. Last, high mean Max and TI-NDVI were associated with fine-textured soils, whereas low mean Max and TI-NDVI were associated with coarse-textured soils. Mean Max and TI-NDVI exhibited slightly different relationships with landscape age. High mean Max NDVI was associated with older landscapes (~70 000 years old), and low mean Max NDVI was associated with younger (~25 000 years old) and recently disturbed landscapes (~1000 years old). Mid-mean TI-NDVI was associated with older landscapes (result not shown), whereas high and low mean TI-NDVI were associated with younger landscapes. Low mean TI-NDVI was also associated with recently disturbed landscapes. Results were similar for analyses run on stratified random samples using 2/3 and 1/2 of the input datasets (table 2).

3.3. Max and TI-NDVI trends

Max and TI-NDVI increased across a majority of the Peninsula between 2001 and 2018 (figure 3). Max NDVI trends were positive across 57.4% of the Peninsula (5.0% significant positive trends [p-value < 0.05]) and negative across 17.8% (0.6% significant negative trends). Additionally, 25.4% of the Peninsula exhibited no Max NDVI trend (p-value > 0.05 and Sen's slope $= 0.000$). Max NDVI Sen's slope ranged from -0.022 to 0.045 yr^{-1}, with the mode between 0.000 and 0.001 yr^{-1}. TI-NDVI trends were positive across 97.6% of the

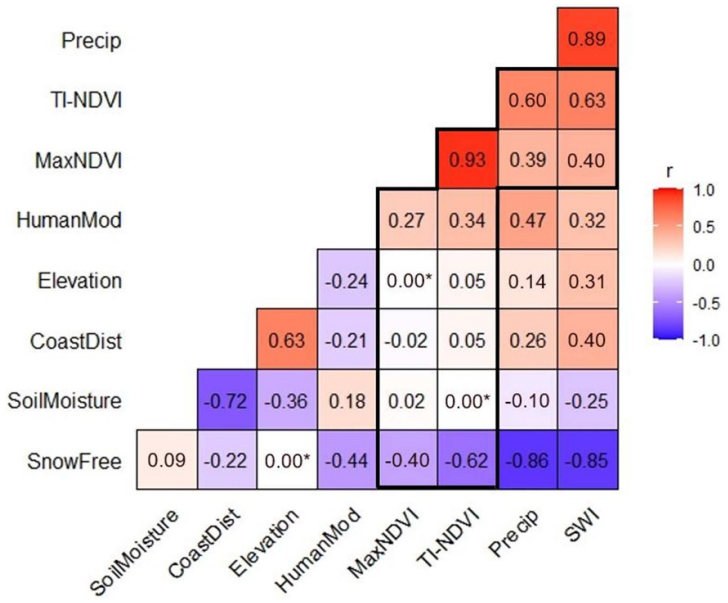

Figure 2. Spearman's correlation coefficients (r) for correlations between Max NDVI, TI-NDVI, and continuous drivers. The 2001–2018 means of Max NDVI, TI-NDVI, precipitation (Precip), snow-free period onset date (SnowFree), soil moisture, and summer warmth index (SWI) were used. Human modification (HumanMod), elevation, and coast distance (CoastDist) values included were constant over the study period. Max and TI-NDVI correlations are highlighted by the thicker black boxes. *Insignificant at the 95% confidence level.

Table 2. Chi-square test of independence results. All tests were significant at the 95% confidence level. Bolded residual values with the largest absolute values had the greatest influence on the spatial associations. Positive residuals indicate a positive relationship and negative residuals indicate a negative relationship. The mid-mean Max and TI-NDVI categories are excluded because the most influential relationships were associated with high and low mean Max and TI-NDVI categories.

Drivers		Chi-square test of independence residuals			
		Mean Max NDVI		Mean TI-NDVI	
		High	Low	High	Low
Vegetation unit	Erect shrub	41.0	−43.8	**72.3**	−66.1
	Graminoid	−30.3	33.5	−66.8	48.2
	Prostrate shrub	−43.5	**49.5**	−57.4	65.1
	Wetland	9.5	−15.9	22.5	−8.6
Substrate chemistry	Acidic	−22.4	15.8	−2.4	17.7
	Circumneutral	**50.7**	−36.5	6.1	**−41.3**
	Saline	−0.9	5.3	−4.7	10.9
Soil texture	Clay loam	7.2	−10.1	7.7	−6.3
	Loam	−2.3	5.1	−11.2	5.2
	Sand	−4.4	8.0	−9.7	12.4
	Sandy loam	**−28.1**	16.5	−30.7	20.6
	Silt loam	18.8	−14.8	**32.0**	−18.5
Landscape age	Older	3.9	−5.6	−2.4	**−28.5**
	Younger	−1.7	2.1	1.1	12.2
	Recently disturbed	−0.9	**7.3**	−0.4	8.9

Note: Bold indicates the most influence on the spatial associations.

Peninsula (13.9% significant positive trends) and negative across 1.9% (<0.1% significant negative trends). Only 0.4% of the Peninsula exhibited no TI-NDVI trend. TI-NDVI Sen's slope ranged from −0.130 to 0.238 yr^{-1}, with the mode between 0.020 and 0.030 yr^{-1}. Overall, 71.5% of the Peninsula exhibited simultaneous increases in Max and TI-NDVI, 1.4% exhibited simultaneous decreases, and 27.1% exhibited divergent trends (figure 4). The direction and magnitude of climatic driver trends were variable (supplemental figure 4).

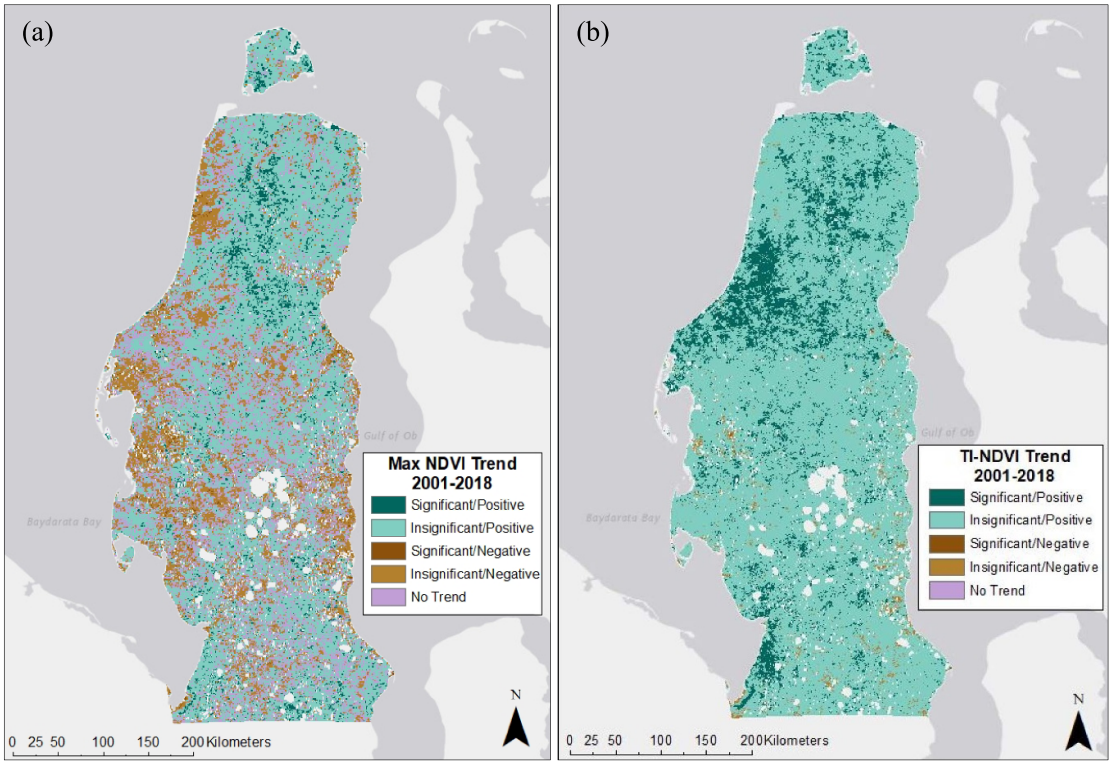

Figure 3. Trends in (a) Max NDVI and (b) TI-NDVI inferred from Mann–Kendall trend tests and Sen's slope estimation. Pixels were classified based on trend significance at the 95% confidence level and Sen's slope direction. Pixels classified as no trend had insignificant trends and Sen's slopes = 0.000. Permanent water bodies and pixels with < 15 years of data (due to low quality data or conditions preventing vegetation growth) were masked.

3.4. Drivers of Max and TI-NDVI trends

The Max NDVI RFR model for the entire Peninsula explained 65% of Max NDVI Sen's slope variance, and the model for areas with significant Max NDVI trends explained 76%. The most important drivers of Max NDVI trends across the Peninsula were coast distance, human modification, soil moisture Sen's slope, precipitation Sen's slope, elevation, and SWI Sen's slope (supplemental figure 5). These were also the most important drivers of significant Max NDVI trends; however, precipitation and SWI trends were better predictors in these areas (supplemental figure 6). Driver relationships with Max NDVI trends were similar across the entire Peninsula and areas that exhibited significant change (supplemental figure 7). Due to the limited spatial extent of significant trends, the results discussion focuses on findings for the entire Peninsula.

On average, positive Max NDVI trends were strongest further inland, at higher elevations, and where SWI trends exceeded approximately 0.5 °C months yr^{-1} (figure 5). However, some strong, positive Max NDVI trends occurred along the southeastern coastline at elevations between −15 m and −13 m (below sea level) (<1.0% of pixels). Additionally, only 1.7% of the Peninsula experienced increases in SWI greater than 0.5 °C months yr^{-1} (equivalent to a cumulative SWI increase of greater than 9 °C months). Prior to reaching this threshold, Max NDVI and SWI trends exhibited a slightly negative relationship. The covariation between detrended Max NDVI and SWI time series was variable, with 53.9% of pixels exhibiting a negative correlation (4.9% significant, p-value < 0.05) and 46.1% exhibiting a positive correlation (3.5% significant) (figure 6).

Positive Max NDVI trends were also strongest where human modification was limited and where soil moisture and precipitation trends were negative (figure 5). Most pixels had less than 3% of their area modified by human activities; however, pixels with 30% or more modified area exhibited negative Max NDVI trends. Detrended Max NDVI and soil moisture time series were negatively correlated across 68.5% of the Peninsula (4.5% significant) and positively correlated across 31.5% (1.5% significant) (figure 7). Similarly, detrended Max NDVI and precipitation time series were negatively correlated across 62.8% of the Peninsula (4.3% significant) and positively correlated across 37.2% (1.6% significant) (supplemental figure 8). These correlations, although spatially variable, indicate that above-average Max NDVI co-occurred with below-average soil moisture and precipitation across a majority of the Peninsula.

The TI-NDVI RFR model for the entire Peninsula explained 70% of TI-NDVI Sen's slope variance, and the model for areas with significant TI-NDVI trends explained 73%. Max and TI-NDVI Sen's slopes (across the Peninsula and where trends were significant) were best predicted by the same six variables; however, the

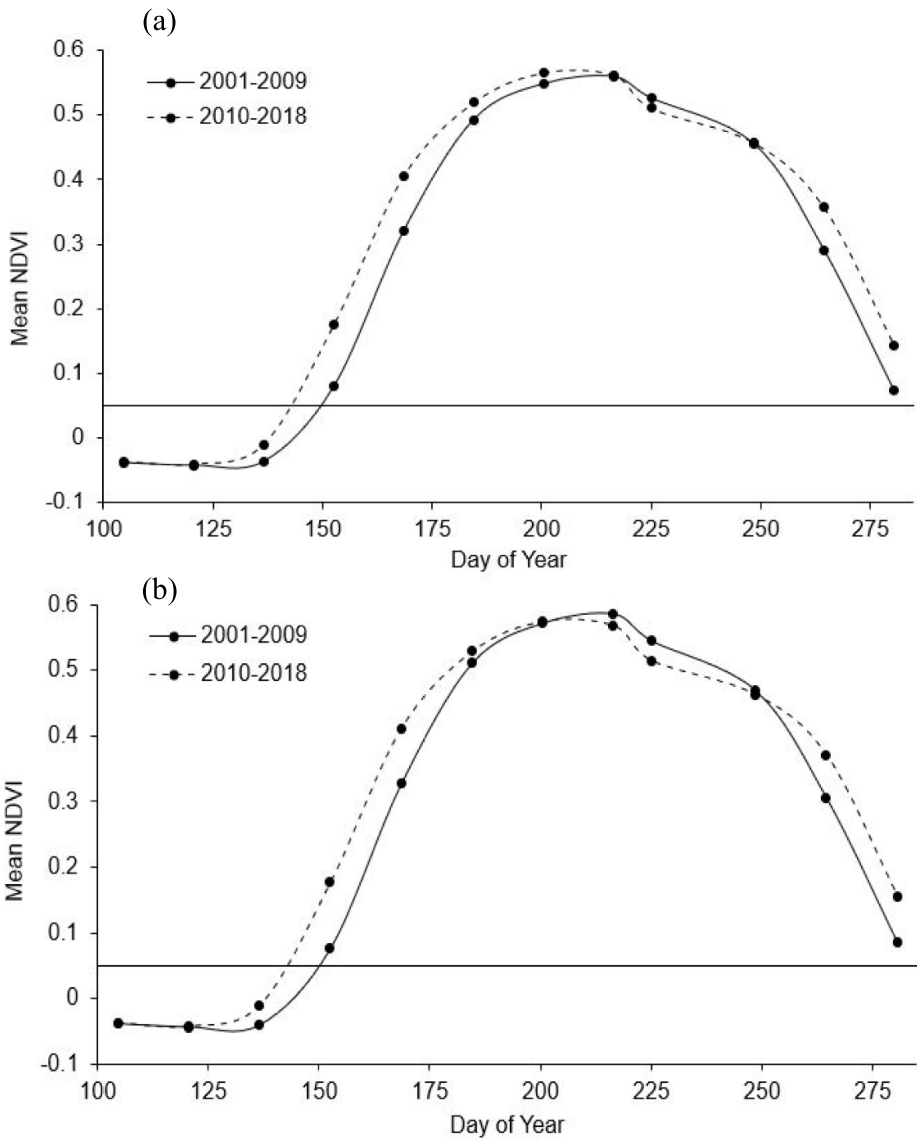

Figure 4. Phenology curves for pixels where (a) Max and TI-NDVI increased and (b) where Max NDVI decreased while TI-NDVI increased. Mean 2001–2009 and 2010–2018 NDVI values were calculated for each 16-day growing season composite image to assess how Max and TI-NDVI shifted between the first and second halves of the study period. Max NDVI is represented by the peak mean NDVI value at the top of each curve, and TI-NDVI is represented by the area under the curve. The line at mean NDVI = 0.05 indicates the minimum threshold for NDVI values included in TI-NDVI calculation.

importance of these variables varied (supplemental figures 5 and 6). The most important drivers of TI-NDVI trends across the Peninsula were coast distance, elevation, precipitation Sen's slope, human modification, SWI Sen's slope, and soil moisture Sen's slope. Human modification and SWI Sen's slope were more important where TI-NDVI trends were significant (supplemental figure 6). Driver relationships with TI-NDVI trends were similar across the entire Peninsula and areas that exhibited significant change, with the exception of soil moisture trends and elevation (supplemental figure 9). Similarly to Max NDVI trends, the results discussion focuses on findings for the entire Peninsula.

On average, positive TI-NDVI trends were strongest at higher elevations, where SWI trends exceeded approximately 0.1 °C months yr^{-1}, and where soil moisture trends were slightly positive around 0.5 mm yr^{-1} (figure 8). The positive relationship between TI-NDVI and SWI trends became stronger after SWI Sen's slopes reached 0.5 °C months yr^{-1}. Detrended TI-NDVI and SWI time series were positively correlated across 99.9% of the Peninsula (78.1% significant), indicating that annual TI-NDVI and SWI positively covaried across nearly the entire Peninsula (figure 9). Positive TI-NDVI trends were consistently stronger where soil moisture Sen's slopes were less negative and approaching 0 mm yr^{-1}. Detrended TI-NDVI and soil moisture time series were negatively correlated across 67.1% of the Peninsula (6.8% significant) and positively correlated across 32.8% (0.7% significant) (figure 10). Therefore, although

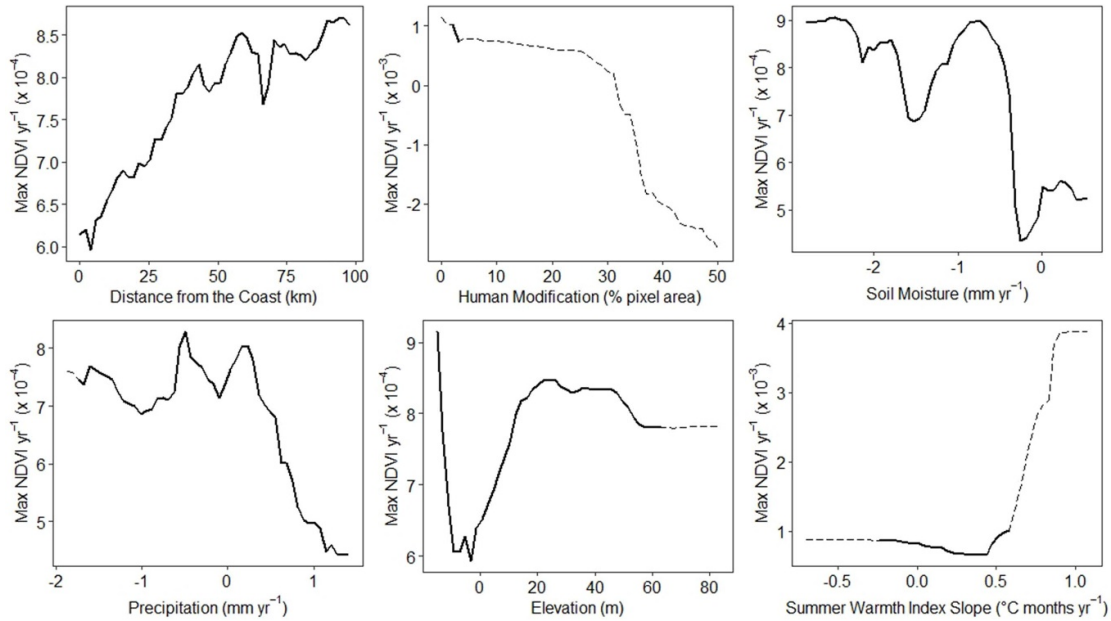

Figure 5. Partial dependence plots for the six most important drivers of Max NDVI Sen's slope across the Peninsula (significant and insignificant trends): distance from the coast, human modification, mean growing season soil moisture Sen's slope, mean growing season precipitation Sen's slope, elevation, and summer warmth index (SWI) Sen's slope. Partial dependence plots display the average predicted relationships between Max NDVI trends and individual drivers across their range of values while still considering the average effects of the other drivers (Goldstein *et al* 2015). Dashed lines indicate outlier driver variable values.

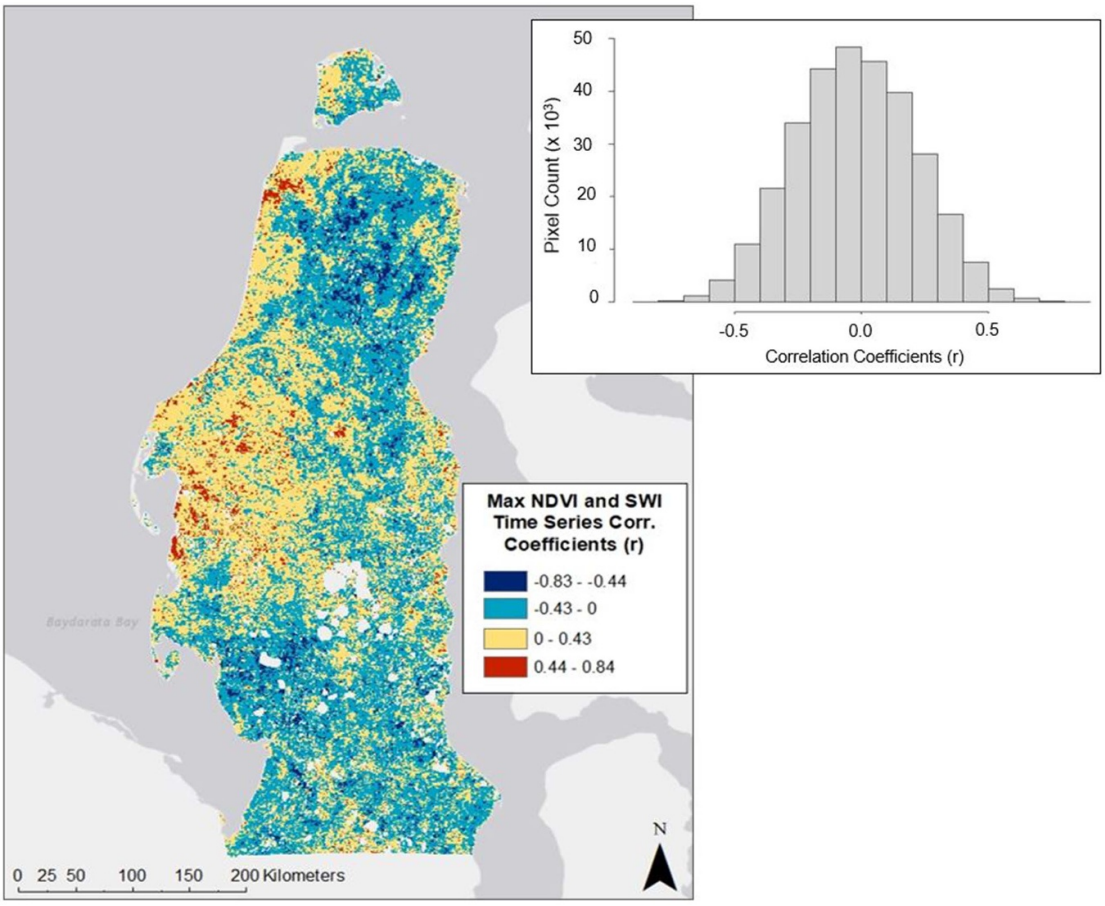

Figure 6. Map of Spearman's correlation coefficients (r) for pixel-wise correlations between linearly detrended Max NDVI and SWI time series (2001–2018). The inset histogram displays the frequency of r values across the Yamal Peninsula.

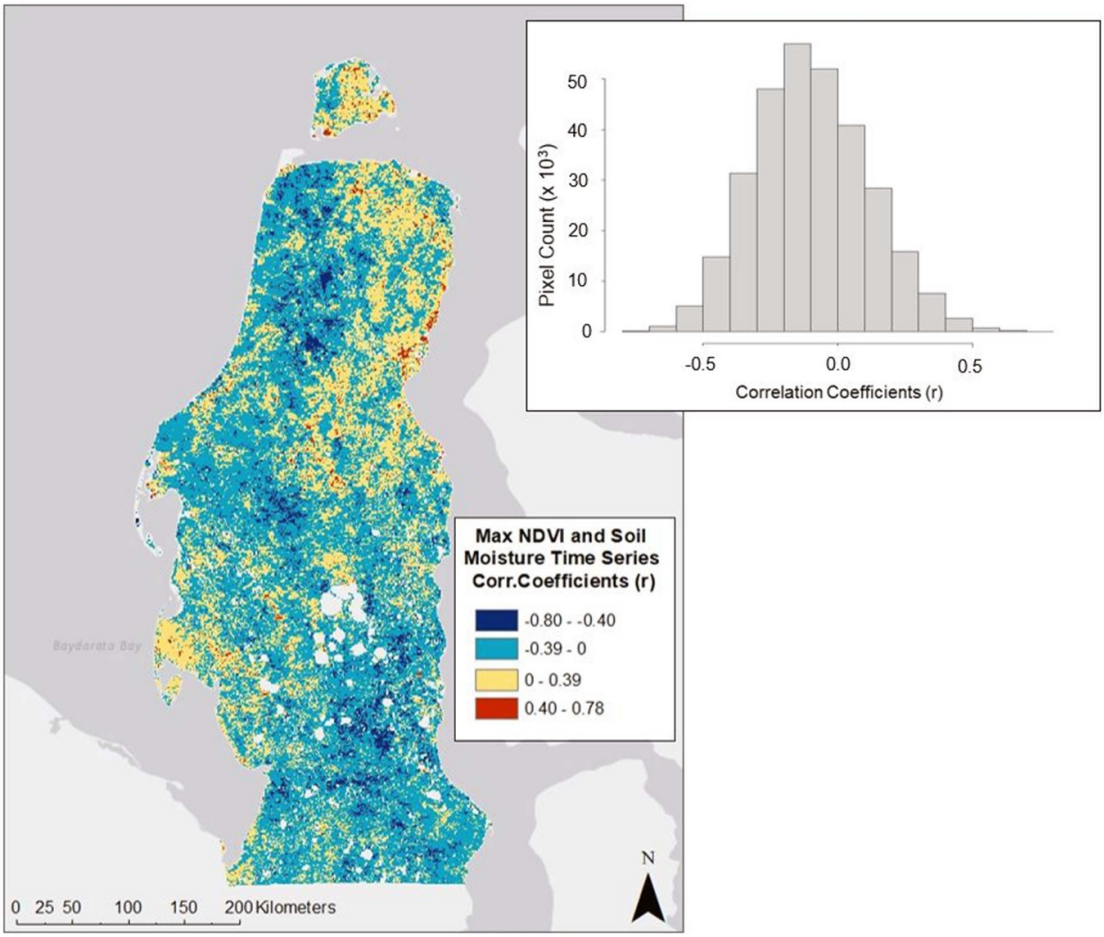

Figure 7. Map of Spearman's correlation coefficients (r) for pixel-wise correlations between linearly detrended Max NDVI and mean growing season soil moisture time series (2001–2018). The inset histogram displays the frequency of r values across the Yamal Peninsula.

TI-NDVI and soil moisture trends exhibited a positive relationship, they did not positively covary interannually across a majority of the Peninsula.

Positive TI-NDVI trends were also strongest closer to the coast, where precipitation trends were negative, and where human modification was limited (figure 8). TI-NDVI trends fluctuated with distance from the coast but were strongest between 0 and 75 km inland. The relationship between TI-NDVI and precipitation trends was unimodal, with the strongest TI-NDVI trends occurring where precipitation decreased by approximately 0.5 mm yr^{-1}. Detrended TI-NDVI and precipitation time series were positively correlated across 76.6% of the Peninsula (1.5% significant) and negatively correlated across 26.3% (<0.1% significant); therefore, TI-NDVI and precipitation positively covaried interannually across a majority of the Peninsula, despite the trends exhibiting a negative relationship where precipitation trends were greater than -0.5 mm yr^{-1} (supplemental figure 10). As with Max NDVI trends, positive TI-NDVI trends were weakest where 30% or more of the area had been modified by humans.

4. Discussion

4.1. Spatial drivers of Max NDVI and TI-NDVI

Climatic drivers and physiognomic vegetation unit best explained the spatial distribution of Max NDVI and TI-NDVI on the Peninsula. On average, areas with higher Max and TI-NDVI coincided with warmer summer temperatures, higher precipitation, earlier snow melt, and vegetation units dominated by erect shrubs and wetland vegetation. Although soil moisture has been found to influence Arctic vegetation distribution (Walker *et al* 2001, Raynolds *et al* 2008, van der Kolk *et al* 2016) and has a more direct effect on water availability than precipitation, it did not exhibit a spatial correlation with Max or TI-NDVI. This implies that the positive spatial correlations among Max/TI-NDVI and precipitation may have been driven by the strong spatial relationships that precipitation has with SWI and snow-free period onset date, rather than spatial patterns of water availability.

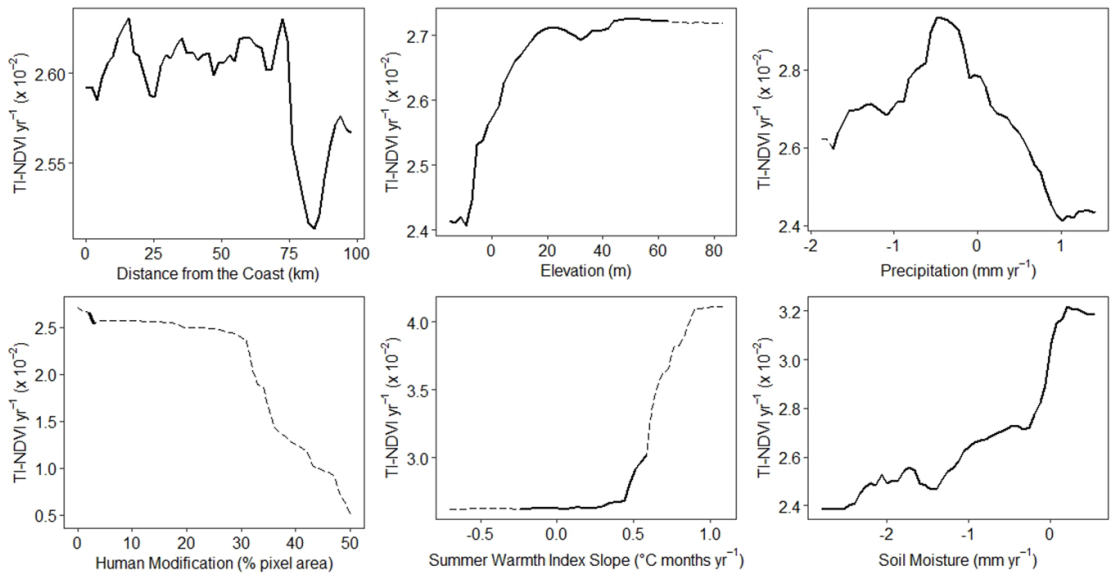

Figure 8. Partial dependence plots for the six most important drivers of TI-NDVI Sen's slope across the Peninsula (significant and insignificant trends): distance from the coast, elevation, mean growing season precipitation Sen's slope, human modification, summer warmth index (SWI) Sen's slope, and mean growing season soil moisture Sen's slope. Partial dependence plots display the average predicted relationships between TI-NDVI trends and individual drivers across their range of values while still considering the average effects of the other drivers (Goldstein *et al* 2015). Dashed lines indicate outlier driver variable values.

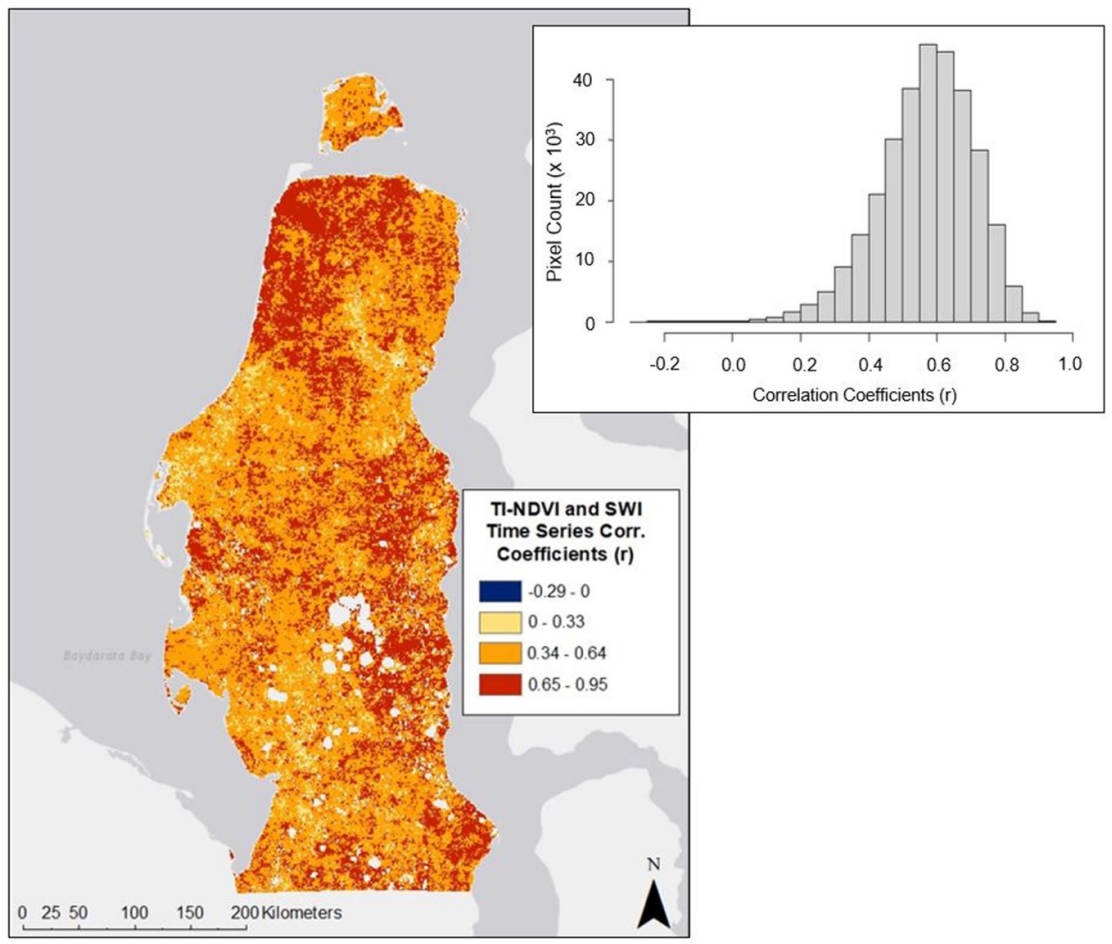

Figure 9. Map of Spearman's correlation coefficients (r) for pixel-wise correlations between linearly detrended TI-NDVI and SWI time series (2001–2018). The inset histogram displays the frequency of r values across the Yamal Peninsula.

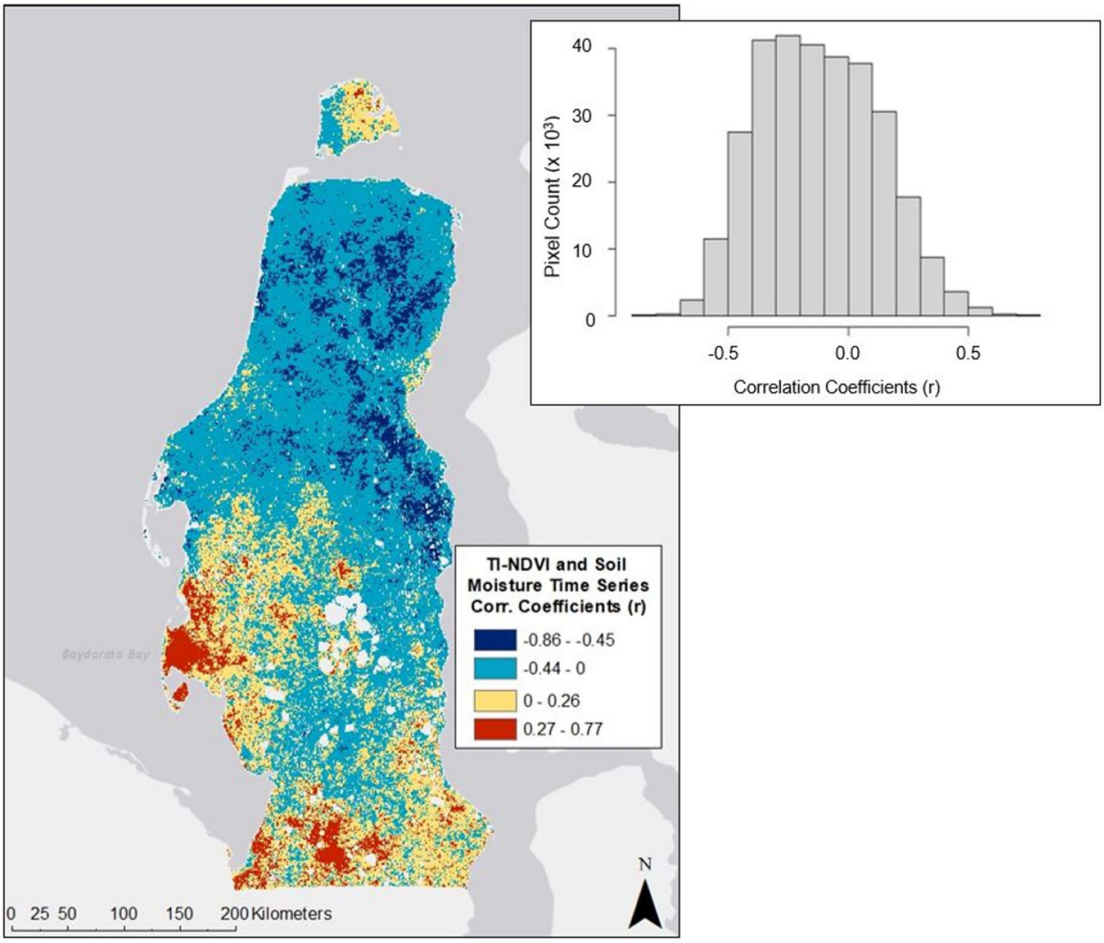

Figure 10. Map of Spearman's correlation coefficients (r) for pixel-wise correlations between linearly detrended TI-NDVI and mean growing season soil moisture time series (2001–2018). The inset histogram displays the frequency of r values across the Yamal Peninsula.

In addition to influencing water availability (Gamon *et al* 2013), the timing of snowmelt determines when the growing season can begin (Bieniek *et al* 2015). Vegetation distribution may have been more limited by summer warmth and growing season onset than water availability because of the continuous permafrost underlying the Peninsula and the mostly shallow active layer depths (Leibman *et al* 2015) that restrict drainage and generally facilitate high soil moisture conditions (Bieniek *et al* 2015). Additionally, our results are consistent with findings that more productive Arctic vegetation with higher aboveground biomass is found where growth is not limited by low temperatures or shorter growing seasons (Jia *et al* 2006, Raynolds *et al* 2006, Epstein *et al* 2021).

The positive spatial correlations between Max/TI-NDVI and human modification were likely the result of warmer, coastal areas with earlier snowmelt also coinciding with more human activity. However, re-vegetated off-road vehicle tracks on the Peninsula near concentrated areas of infrastructure have been found to have higher aboveground biomass than surrounding undisturbed areas approximately 20 years after revegetation (Forbes *et al* 2009). Ground verification and/or comparison with finer resolution imagery would be needed to confirm if this occurred in other re-vegetated areas that were previously impacted by human activities.

Although less important than vegetation unit, substrate chemistry, soil texture, and landscape age also influenced spatial patterns of Max NDVI and TI-NDVI. Max and TI-NDVI were highest on nutrient-rich circumneutral substrates and fine-textured soils, similar to other studies from the region (Walker *et al* 2005, Macias-Fauria *et al* 2012, Epstein *et al* 2021). The weak positive association between high TI-NDVI and younger landscapes was unexpected because older landscapes can have greater nutrient availability and erect shrub coverage after the development of fine-grained soils and stream networks, vegetation succession, and peat accumulation (Walker *et al* 1995). However, the negative spatial association between high TI-NDVI and younger landscapes was stronger and drove the significance of the spatial relationship between TI-NDVI and landscape age.

4.2. Max and TI-NDVI trends

Max NDVI and TI-NDVI increased across a majority of the Peninsula between 2001 and 2018. The magnitude and direction of the trends were spatially variable, with most pixels exhibiting insignificant change. Max NDVI has consistently increased across a majority of the Peninsula for the past three decades, while the nearly uniform increase in TI-NDVI indicates a recent shift from negative to positive TI-NDVI trends in some areas (Bhatt *et al* 2021). The co-occurrence of negative Max NDVI and positive TI-NDVI trends could be explained by the different aspects of productivity and phenology that these variables represent (figures 3 and 4). Max NDVI better identifies the contribution of the growth form with the greatest aboveground biomass at the peak of the snow-free season (erect shrubs across a majority of the Peninsula) compared to TI-NDVI, which better captures the contributions of all growth forms to snow-free season productivity (Jia *et al* 2006, Bhatt *et al* 2021). Therefore, areas with negative Max NDVI and positive TI-NDVI trends potentially experienced total productivity increases despite decreases in peak erect shrub biomass due to the expansion of graminoids and/or increased growing season length (van der Kolk *et al* 2016, Magnússon *et al* 2021). This shift in community composition has been reported for the central Peninsula following disturbances from off-road vehicle tracks and heavy reindeer grazing (Forbes *et al* 2009, Kumpula *et al* 2011), but could not be confirmed for other areas without ground verification.

4.3. Drivers of Max NDVI and TI-NDVI trends

The best predictors of Max NDVI and TI-NDVI trends were a combination of geomorphic (coast distance and elevation), anthropogenic (human modification), and climatic (precipitation trends, soil moisture trends, and SWI trends) drivers. Coast distance was the best predictor of Max and TI-NDVI trends across the entire Peninsula and in areas that exhibited significant trends. Positive Max and TI-NDVI trends across the Peninsula exhibited similar relationships with precipitation trends, elevation, and human modification but had opposing relationships with coast distance, soil moisture trends, and SWI trends less than 0.5 °C months yr^{-1}. These relationships could be due to erect shrubs and other growth forms having differential responses to some drivers and coordinated responses to others. While these findings elucidate the relationships between positive Max/TI-NDVI trends and their drivers, they also provide insight into the potential causes of divergent Max and TI-NDVI trends.

Coast distance captures the effect of coastal-inland gradients in SWI on the Peninsula (figure 2). The consistently cooler coastal temperatures influenced by sea ice (Bhatt *et al* 2010) and maritime airflow (Bhatt *et al* 2021) potentially facilitated graminoid, forb, moss, and lichen growth (indicated by stronger positive TI-NDVI trends) and limited shrub growth (indicated by weaker positive Max NDVI trends) (Walker *et al* 2005). As coastal temperatures increase due to melting sea ice (Bhatt *et al* 2021), shrub growth may become less limited near the Peninsula's coastline. The negative spatial relationship between coast distance and mean soil moisture may also indicate the influence of nutrient availability on the Peninsula's vegetation productivity trends (figure 2). Graminoids are able to take advantage of low nutrients in high soil moisture conditions that can limit shrub growth (van der Kolk *et al* 2016), and soil organic nitrogen content may limit increased shrub growth in response to warming on the Peninsula (Yu *et al* 2011). Additionally, limited shrub growth along the coast would facilitate moss and lichen growth by decreasing light competition and burial under litter (van Wijk *et al* 2004).

The opposing relationships between Max/TI-NDVI trends, soil moisture trends, and SWI trends indicate that climate-induced permafrost degradation may have driven moisture regime shifts that favored shrub growth and positive Max NDVI trends where drying was more pronounced, but graminoid, forb, and moss growth and positive TI-NDVI trends where drying was less pronounced or wetting occurred (van der Kolk *et al* 2016, Jorgenson *et al* 2022). However, significant positive TI-NDVI trends (13.9% of the Peninsula) were found to be stronger where soil moisture had decreased. Warming has been found to increase shrub, graminoid, and forb growth (Walker 2006, Elmendorf *et al* 2012) and would be expected to have a positive relationship with Max and TI-NDVI trends without the influence of other limiting factors (Berner *et al* 2020). Prior to reaching the 0.5 °C months yr^{-1} threshold that resulted in the strongest positive relationships between Max/TI-NDVI trends and SWI trends, the influence of positive SWI trends on permafrost thaw and subsequent soil moisture conditions was likely more important than their direct effects on vegetation growth. Ice wedge degradation and the expansion of thermokarst features (lakes, gullies, and pits) facilitate wetting that can cause shrub death and the succession of graminoids, forbs, and mosses (Magnússon *et al* 2021, Jorgenson *et al* 2022). Conversely, thermokarst that causes lake drainage and the drying of areas adjacent to depressions could contribute to strong negative soil moisture trends that favored shrub growth (Loiko *et al* 2020, Jin *et al* 2021). Ice wedges, thermokarst features, and drained thermokarst lakes are abundant on the Peninsula (Leibman *et al* 2014), and these processes have been reported elsewhere in the Eurasian (Frost and Epstein 2014, Loiko *et al* 2020, Magnússon *et al* 2021) and North American (Jorgenson *et al* 2015, Lantz 2017) Arctic. However, further research using in situ or high-resolution remote

measurements of these processes is needed to confirm their influence on the Peninsula's Max NDVI and TI-NDVI trends. The negative relationships between positive Max NDVI trends/significantly positive TI-NDVI trends and soil moisture trends could be the result of spectral contamination within pixels with high soil moisture (Myers-Smith *et al* 2020); however, we would have expected a similar impact on the Peninsula-wide TI-NDVI trend relationship if this were the case.

Increasing precipitation has been found to benefit graminoid growth over shrub growth in mixed vegetation communities (van der Kolk *et al* 2016); however, positive Max and TI-NDVI trends had a negative relationship with precipitation trends. These similar relationships could have been associated with the effect of precipitation on the frequency of cryogenic landslides (Leibman *et al* 2014) and/or an increase in early growing season rain-on-snow events (Phoenix and Bjerke 2016). Increased precipitation is the primary cause of cryogenic landslides (Leibman *et al* 2014) that result in shear surfaces that remain sparsely vegetated for decades before recolonization by shrubs (Walker *et al* 2009, Verdonen *et al* 2020). Additionally, April rain-on-snow events followed by below-freezing temperatures have been recorded on the Peninsula during the study period (Bartsch *et al* 2010) and can result in the death of vegetation due to ice encasement and the formation of ice crusts (Phoenix and Bjerke 2016).

4.4. Interannual covariation between Max NDVI, TI-NDVI, and climatic drivers

The degree of positive or negative interannual covariation between Max/TI-NDVI and climatic drivers provided insight into the more immediate responses of vegetation to fluctuating conditions that may or may not be reflected by the average trend relationships (Myers-Smith *et al* 2020). The positive correlation between annual TI-NDVI and SWI across 99.9% of the Peninsula indicates that total growing season productivity consistently fluctuated with SWI between 2001 and 2018. However, the SWI trend was not the most important driver of the trend in total growing season productivity across the Peninsula or in areas that exhibited significant change. Additionally, detrended TI-NDVI and precipitation were positively correlated across 74.0% of the Peninsula, but positive TI-NDVI trends had a negative relationship with precipitation trends greater than -0.5 mm yr^{-1}. Higher precipitation during any given year could have immediate beneficial effects on TI-NDVI by limiting water stress (Opala-Owczarek *et al* 2018), whereas increases in precipitation over time could cause an increase in landslides (Leibman *et al* 2014) and/or early growing season rain-on-snow events (Phoenix and Bjerke 2016) that would weaken positive TI-NDVI trends. Overall, the correlations among Max/TI-NDVI and SWI, soil moisture, and precipitation detrended time series revealed concentrated areas of strong positive and negative covariation occurring throughout the Peninsula. This heterogeneity is reflective of the spatiotemporal variation in the suite of drivers that influence Arctic vegetation productivity, and highlights the difficulty in generalizing the effects of individual drivers on Arctic vegetation productivity across large regions.

5. Summary and conclusions

These findings indicate that spatial patterns of Max and TI-NDVI were similarly influenced by SWI, growing season onset, and vegetation type whereas Max and TI-NDVI trends had variable relationships with drivers and were primarily influenced by coastal-inland gradients in SWI and soil moisture. Max and TI-NDVI increased across a majority of the Peninsula between 2001 and 2018, and TI-NDVI trends may have recently shifted from negative to positive in some areas (Bhatt *et al* 2021) despite some concurrent decreases in Max NDVI. The best predictors of change in Max and TI-NDVI trends were the same for the entire Peninsula and areas of significant change, and a majority of the driver-trend relationships were similar. The significant TI-NDVI trend-driver relationships that differed (soil moisture trends and elevation) could be reflective of conditions in the areas where they were concentrated along the northwest and southwest coastlines. Relationships among Max/TI-NDVI trends and climatic driver trends pointed to the potential influence of permafrost degradation on Max and TI-NDVI via changes in hydrological conditions. Further, the negative relationships between Max/TI-NDVI trends and human modification indicate that anthropogenic disturbances are becoming an increasingly important mediator of vegetation responses to changing climate and landscape conditions as development of the Peninsula intensifies (Walker *et al* 2009, 2022).

The coarse resolution (1 km) imagery used in this study captures the dominant landscape features of an area rather than the sub-pixel heterogeneity that exists on the ground. This aggregation of features can introduce uncertainty in the relationships between NDVI metrics and environmental drivers (Myers-Smith *et al* 2020), but allows for the assessment of the broader scale controls across expansive Arctic landscapes such as the Peninsula. Remote sensing analyses using coarse resolution imagery can also miss the impact of fine-scale landscape features related to permafrost degradation (Myers-Smith *et al* 2020); however, the comparison of Max and TI-NDVI trend relationships indicated that permafrost processes may be causing differential vegetation responses and divergent trends. Divergent trends were likely caused by a shift from

shrub to graminoid dominance which can occur following permafrost thaw, landslides (Magnússon *et al* 2021), and heavy reindeer grazing (Forbes *et al* 2009). While this study focused on the spatial and temporal drivers of Max and TI-NDVI and did not directly assess aboveground biomass, the strong relationship between aboveground biomass and these NDVI metrics at coarse resolutions (Raynolds *et al* 2012, Jia *et al* 2006) allowed for inferences into how broad-scale aboveground biomass changes influenced the observed Max and TI-NDVI driver relationships. Additional research detailing the interaction between permafrost degradation and reindeer herbivory is needed to determine their combined effects on the Peninsula's Max NDVI and TI-NDVI.

Arctic Max NDVI and TI-NDVI have continued to increase since 2018; however, so has trend variability as climate and landscape changes result in differential ecosystem impacts (Bhatt *et al* 2021, Frost *et al* 2022). This study provides insight into the potential future of Arctic regions undergoing warming, moisture regime shifts, and increasing human modification, and demonstrates the usefulness of considering multiple NDVI metrics to disentangle the effects of individual drivers across heterogeneous landscapes.

Data availability statement

All data that support the findings of this study are included within the article (and any supplementary information files).

Acknowledgments

This work was funded by the NASA Biodiversity and Ecological Forecasting Programs (Grant 80NSSC18K0446) and was affiliated with the NASA Arctic Boreal Vulnerability Experiment (ABoVE). We thank Dr Xi Yang and Dr Lauren Simkins for helpful discussions and early revisions to the manuscript. We thank the University of Virginia's Research Computing team for their programming support.

ORCID iDs

Morgan S Tassone https://orcid.org/0009-0008-9863-4197
Howard E Epstein https://orcid.org/0000-0003-2817-4486
Amanda H Armstrong https://orcid.org/0000-0002-9123-8924
Uma S Bhatt https://orcid.org/0000-0003-1056-3686
Gerald V Frost https://orcid.org/0000-0002-5134-0334
Birgit Heim https://orcid.org/0000-0003-2614-9391

References

Abatzoglou J T, Dobrowski S Z, Parks S A and Hegewisch K C 2018 TerraClimate, a high-resolution global dataset of monthly climate and climatic water balance from 1958–2015 *Sci. Data* **5** 170191

Armstrong A, Tassone M and Braaten J 2022 Defining seasonality: first date of no snow *Cloud-Based Remote Sensing with Google Earth Engine: Fundamentals & Applications* ed Cardille, Clinton, Crowley and Saah (Springer) ch A2.6, pp 133–51 (available at: www.eefabook.org/)

Bartsch A, Kumpula T, Forbes B C and Stammler F 2010 Detection of snow surface thawing and refreezing in the Eurasian Arctic with QuikSCAT: implications for reindeer herding *Ecol. Appl.* **20** 2346–58

Berner L T *et al* 2020 Summer warming explains widespread but not uniform greening in the Arctic tundra biome *Nat. Commun.* **11** 4621

Bhatt U S *et al* 2010 Circumpolar arctic tundra vegetation change is linked to sea ice decline *Earth Interact.* **14** 1–20

Bhatt U S *et al* 2021 Climate drivers of Arctic tundra variability and change using an indicators framework *Environ. Res. Lett.* **16** 055019

Bieniek P A *et al* 2015 Climate drivers linked to changing seasonality of Alaska Coastal Tundra vegetation productivity *Earth Interact.* **19** 1–29

Blok D, Heijmans M M P D, Schaepman-Strub G, Kononov A V, Maximov T C and Berendse F 2010 Shrub expansion may reduce summer permafrost thaw in Siberian tundra *Glob. Change Biol.* **16** 1296–305

Borchers H W 2019 Pracma: practical numerical math functions. R package version 2.2.9 (available at: https://CRAN.R-project.org/package=pracma)

Cunliffe A M, J Assmann J, N Daskalova G, Kerby J T and Myers-Smith I H 2020 Aboveground biomass corresponds strongly with drone-derived canopy height but weakly with greenness (NDVI) in a shrub tundra landscape *Environ. Res. Lett.* **15** 125004

Didan K 2015 MOD13Q1 MODIS/terra vegetation indices 16-day L3 *Global 250m SIN Grid V006* (https://doi.org/10.5067/MODIS/MOD13Q1.006)

Dutrieux L P, Bartholomeus H, Herold M and Verbesselt J 2012 Relationships between declining summer sea ice, increasing temperatures and changing vegetation in the Siberian Arctic tundra from MODIS time series (2000–11) *Environ. Res. Lett.* **7** 044028

Elmendorf S C *et al* 2012 Plot-scale evidence of tundra vegetation change and links to recent summer warming *Nat. Clim. Change* **2** 453–7

Epstein H E *et al* 2021 Spatial patterns of arctic tundra vegetation properties on different soils along the Eurasia Arctic Transect, and insights for a changing Arctic *Environ. Res. Lett.* **16** 014008

Epstein H E, Beringer J, Gould W A, Lloyd A H, Thompson C D, Chapin F S, Michaelson G J, Ping C L, Rupp T S and Walker D A 2004 The nature of spatial transitions in the Arctic *J. Biogeogr.* **31** 1917–33
Epstein H E, Raynolds M K, Walker D A, Bhatt U S, Tucker C J and Pinzon J E 2012 Dynamics of aboveground phytomass of the circumpolar Arctic tundra during the past three decades *Environ. Res. Lett.* **7** 015506
(ESA) and université catholique de louvain (UC Louvain) 2010 *GlobCover 2009* (available at: http://due.esrin.esa.int/page_globcover.php)
FAO/IIASA/ISRIC/ISS-CAS/JRC 2012 *Harmonized World Soil Database (Version 1.2)* (FAO)
Forbes B C 1999 Land use and climate change on the Yamal Peninsula of north-west Siberia: some ecological and socio-economic implications *Polar Res.* **18** 367–73
Forbes B C and Kumpula T 2009 The ecological role and geography of reindeer (Rangifer tarandus) in Northern Eurasia: ecology/geography of Eurasian reindeer *Geogr. Compass* **3** 1356–80
Forbes B C, Stammler F, Kumpula T, Meschtyb N, Pajunen A and Kaarlejärvi E 2009 High resilience in the Yamal-Nenets social–ecological system, West Siberian Arctic, Russia *Proc. Natl Acad. Sci.* **106** 22041–8
Fox J and Weisberg S 2019 *An R Companion to Applied Regression, Third Edition* (Sage)
Frost G V *et al* 2020 *Tundra Greenness in Arctic Report Card Update for 2020* (National Oceanic and Atmospheric Administration) (https://doi.org/10.25923/46rm-0w23)
Frost G V *et al* 2021 *Tundra Greenness in Arctic Report Card Update for 2021* (National Oceanic and Atmospheric Administration) (https://doi.org/10.25923/8n78-wp73)
Frost G V *et al* 2022 *Tundra Greenness in Arctic Report Card Update for 2022* (National Oceanic and Atmospheric Administration) (https://doi.org/10.25923/g8w3-6v31)
Frost G V and Epstein H E 2014 Tall shrub and tree expansion in Siberian tundra ecotones since the 1960s *Glob. Change Biol.* **20** 1264–77
Gamon J A, Huemmrich K F, Stone R S and Tweedie C E 2013 Spatial and temporal variation in primary productivity (NDVI) of coastal Alaskan tundra: decreased vegetation growth following earlier snowmelt *Remote Sens. Environ.* **129** 144–53
Gazprom 2021 Yamal (available at: www.gazprom.com/projects/yamal/)
Goldstein A, Kapelner A, Bleich J and Pitkin E 2015 Peeking inside the black box: visualizing statistical learning with plots of individual conditional expectation *J. Comput. Graph. Stat.* **24** 44–65
Greenwell B M 2017 pdp: an R package for constructing partial dependence plots *R J.* **9** 421–36
Hall D K *et al* 2016 *MODIS/Terra Snow Cover Daily L3 Global 500m Grid Version 6* (NASA National Snow and Ice Data Center Distributed Active Archive Center)
Hijmans R J 2021 terra: spatial data analysis R package version 1.0–10 (available at: https://CRAN.R-project.org/package=terra)
IPCC 2021 Climate change 2021: the physical science basis *Contribution of Working Group I to the Sixth Assessment Report of the Intergovernmental Panel on Climate Change* (Cambridge University Press)
Jia G J, Epstein H E and Walker D A 2006 Spatial heterogeneity of tundra vegetation response to recent temperature changes *Glob. Change Biol.* **12** 42–55
Jin X Y, Jin H J, Iwahana G, Marchenko S S, Luo D L, Li X Y and Liang S H 2021 Impacts of climate-induced permafrost degradation on vegetation: a review *Adv. Clim. Change Res.* **12** 29–47
Jorgenson M T *et al* 2022 Rapid transformation of tundra ecosystems from ice-wedge degradation *Glob. Planet. Change* **216** 103921
Jorgenson M T, Kanevskiy M, Shur Y, Moskalenko N, Brown D R N, Wickland K, Striegl R and Koch J 2015 Role of ground ice dynamics and ecological feedbacks in recent ice wedge degradation and stabilization *J. Geophys. Res. Earth Surf.* **120** 2280–97
Kennedy C M, Oakleaf J R, Theobald D M, Baruch-Mordo S and Kiesecker J 2019 Managing the middle: a shift in conservation priorities based on the global human modification gradient *Glob. Change Biol.* **25** 811–26
Kuhn M 2020 Caret: classification and regression training R package version 6.0–86 (available at: https://CRAN.R-project.org/package=caret)
Kulkarni A and Storch H V 1995 Monte Carlo experiments on the effect of serial correlation on the Mann-Kendall test of trend *Kurzberichte* **4** 82–85
Kumpula T, Pajunen A, Kaarlejarvi E, Forbes B C and Stammler F 2011 Land use and land cover change in Arctic Russia: ecological and social implications of industrial development *Glob. Environ. Change* **21** 550–62
Lantz T C 2017 Vegetation succession and environmental conditions following catastrophic lake drainage in old crow flats, Yukon *ARCTIC* **70** 177
Lara M J, Nitze I, Grosse G, Martin P and McGuire A D 2018 Reduced arctic tundra productivity linked with landform and climate change interactions *Sci. Rep.* **8** 2345
Leibman M O 1995 Cryogenic landslides on the Yamal Peninsula, Russia: preliminary observations *Permafr. Periglac.* **6** 259–64
Leibman M O, Khomutov A, Gubarkov A, Mullanurov D and Dvornikov Y 2015 The research station "Vaskiny Dachi", Central Yamal, West Siberia, Russia—a review of 25 years of permafrost studies *Fennia* **193** 3–30
Leibman M O, Khomutov A and Kizyakov A 2014 Cryogenic landslides in the West-Siberian plain of Russia: classification, mechanisms, and landforms *Landslides in Cold Regions in the Context of Climate Change* ed W Shan, Y Guo, F Wang, H Marui and A Strom (Springer International Publishing) pp 143–62
Liaw A and Wiener M 2002 Classification and regression by randomForest *R News* **2** 18–22
Loiko S, Klimova N, Kuzmina D and Pokrovsky O 2020 Lake drainage in permafrost regions produces variable plant communities of high biomass and productivity *Plants* **9** 867
Macias-Fauria M, Forbes B C, Zetterberg P and Kumpula T 2012 Eurasian Arctic greening reveals teleconnections and the potential for structurally novel ecosystems *Nat. Clim. Change* **2** 613–8
Magnússon R Í, Limpens J, Kleijn D, van Huissteden K, Maximov T C, Lobry S and Heijmans M M P D 2021 Shrub decline and expansion of wetland vegetation revealed by very high resolution land cover change detection in the Siberian lowland tundra *Sci. Total Environ.* **782** 146877
McLeod A I 2011 Kendall: Kendall rank correlation and Mann-Kendall trend test R package version 2.2 (available at: https://CRAN.R-project.org/package=Kendall)
Microsoft Corporation (Microsoft) and Weston S 2020 doParallel: foreach parallel adaptor for the 'parallel' package R package version 1.0.16 (available at: https://CRAN.R-project.org/package=doParallel)
Myers-Smith I H *et al* 2020 Complexity revealed in the greening of the Arctic *Nat. Clim. Change* **10** 106–17
Oliveira S, Oehler F, San-Miguel-Ayanz J, Camia A and Pereira J M C 2012 Modeling spatial patterns of fire occurrence in Mediterranean Europe using multiple regression and random forest *For. Ecol. Manage.* **275** 117–29

Opala-Owczarek M, Pirożnikow E, Owczarek P, Szymański W, Luks B, Kępski D, Szymanowski M, Wojtuń B and Migała K 2018 The influence of abiotic factors on the growth of two vascular plant species (Saxifraga oppositifolia and Salix polaris) in the High Arctic *Catena* **163** 219–32

Patakamuri S K and O'Brien N 2020 modifiedmk: modified versions of mann kendall and spearman's rho trend tests R package version 1.5.0 (available at: https://CRAN.R-project.org/package=modifiedmk)

Pearson R G, Phillips S J, Loranty M M, Beck P S A, Damoulas T, Knight S J and Goetz S J 2013 Shifts in Arctic vegetation and associated feedbacks under climate change *Nat. Clim. Change* **3** 673–7

Phoenix G K and Bjerke J W 2016 Arctic browning: extreme events and trends reversing arctic greening *Glob. Change Biol.* **22** 2960–2

Pohlert T 2020 trend: non-parametric trend tests and change-point detection R package version 1.1.2 (https://doi.org/10.1007/s11356-019-07314-0)

R Core Team 2020 *R: A Language and Environment for Statistical Computing* (R Foundation for Statistical Computing)

Rabosky D L, Grundler M, Anderson C, Title P, Shi J J, Brown J W, Huang H and Larson J G 2014 BAMMtools: an R package for the analysis of evolutionary dynamics on phylogenetic trees *Methods Ecol. Evol.* **5** 701–7

Raynolds M K, Walker D A, Epstein H E, Pinzon J E and Tucker C J 2012 A new estimate of tundra-biome phytomass from trans-Arctic field data and AVHRR NDVI *Remote Sens. Lett.* **3** 403–11

Raynolds M K, Walker D A and Maier H A 2006 NDVI patterns and phytomass distribution in the circumpolar Arctic *Remote Sens. Environ.* **102** 271–81

Raynolds M, Comiso J, Walker D and Verbyla D 2008 Relationship between satellite-derived land surface temperatures, arctic vegetation types, and NDVI *Remote Sens. Environ.* **112** 1884–94

Reichle L M, Epstein H E, Bhatt U S, Raynolds M K and Walker D A 2018 Spatial heterogeneity of the temporal dynamics of arctic tundra vegetation *Geophys. Res. Lett.* **45** 9206–15

Revelle W 2020 psych: procedures for personality and psychological research (Northwestern University) (available at: https://CRAN.R-project.org/package=psychVersion=2.0.9)

Rizzoli P *et al* 2017 Generation and performance assessment of the global TanDEM-X digital elevation model *ISPRS J. Photogramm. Remote Sens.* **132** 119–39

van der Kolk H J, Heijmans M M P D, van Huissteden J, Pullens J W M and Berendse F 2016 Potential Arctic tundra vegetation shifts in response to changing temperature, precipitation and permafrost thaw *Biogeosciences* **13** 6229–45

van Wijk M T *et al* 2004 Long-term ecosystem level experiments at Toolik Lake, Alaska, and at Abisko, Northern Sweden: generalizations and differences in ecosystem and plant type responses to global change *Glob. Change Biol.* **10** 105–23

Verdonen M, Berner L T, Forbes B C and Kumpula T 2020 Periglacial vegetation dynamics in Arctic Russia: decadal analysis of tundra regeneration on landslides with time series satellite imagery *Environ. Res. Lett.* **15** 105020

Walker D A *et al* 2005 The circumpolar Arctic vegetation map *J. Veg. Sci.* **16** 267–82

Walker D A *et al* 2009 Spatial and temporal patterns of greenness on the Yamal Peninsula, Russia: interactions of ecological and social factors affecting the Arctic normalized difference vegetation index *Environ. Res. Lett.* **4** 045004

Walker D A *et al* 2022 Cumulative impacts of a gravel road and climate change in an ice-wedge-polygon landscape, Prudhoe Bay, Alaska *Arct. Sci.* **8** 1040–66

Walker D A, Auerbach N A and Shippert M M 1995 NDVI, biomass, and landscape evolution of glaciated terrain in northern Alaska *Polar Rec.* **31** 169–78

Walker D A, Bockheim J G, Chapin F S, Eugster W, Nelson F E and Ping C L 2001 Calcium-rich tundra, wildlife, and the Mammoth Steppe *Quat. Sci. Rev.* **20** 149–63

Walker D A 2010 Cumulative effects of rapid land-cover and land-use changes on the Yamal Peninsula, Russia *Eurasian Arctic Land Cover and Land Use in a Changing Climate* ed G Gutman and A Reissell (Springer Netherlands) pp 207–36

Walker D A, Gould W A, Maier H A and Raynolds M K 2002 The circumpolar arctic vegetation map: AVHRR-derived base maps, environmental controls, and integrated mapping procedures *Int. J. Remote Sens.* **23** 4551–70

Walker D A and Raynolds M K 2018 *Circumpolar Arctic Vegetation, Geobotanical, Physiographic Maps, 1982–2003* (ORNL DAAC)

Walker M D 2006 Plant community responses to experimental warming across the tundra biome *Proc. Natl Acad. Sci.* **103** 1342–6

Wan Z, Hook S and Hulley G 2015 MOD11A1 MODIS/terra land surface temperature/emissivity daily L3 global 1km SIN grid V006 (NASA EOSDIS land processes DAAC) (available at: https://lpdaac.usgs.gov/products/mod11a1v061/)

Yu Q, Epstein H E, Engstrom R and Walker D A 2017 Circumpolar arctic tundra biomass and productivity dynamics in response to projected climate change and herbivory *Glob. Change Biol.* **23** 3895–907

Yu Q, Epstein H E, Walker D A, Frost G V and Forbes B C 2011 Modeling dynamics of tundra plant communities on the Yamal Peninsula, Russia, in response to climate change and grazing pressure *Environ. Res. Lett.* **6** 045505